

# Shrinkage behaviour of material extrusion steel 316L: influence of primary 3D printing parameters

Solomon O. Obadimu

School of Engineering, University of Limerick, Limerick, Ireland, and

Kyriakos I. Kourousis

School of Engineering, University of Limerick, Limerick, Ireland and CONFIRM Smart Manufacturing Research Centre, Limerick, Ireland

## Abstract

**Purpose** – The wide application of metal material extrusion (MEX) has been hampered by the practicalities associated with the resulting shrinkage of the final parts when commercial three-dimensional (3D) printing equipment is used. The shrinkage behaviour of MEX metal parts is a very important aspect of the MEX metal production process, as the parts must be accurately oversized to compensate for shrinkage. This paper aims to investigate the influence of primary 3D printing parameters, namely, print speed, layer height and print angle, on the shrinkage behaviour of MEX Steel 316L parts.

**Design/methodology/approach** – Two groups of dog-bone and rectangular-shape specimens were produced with the BASF Ultrafuse Steel 316L metal filament. The length, width and thickness of the specimens were measured pre- and post-debinding and sintering to calculate the percentile shrinkage rates. Analysis of variance (ANOVA) was used to evaluate and rank the significance of each manufacturing parameter on shrinkage. Typical main print quality issues experienced in this analysis are also reported.

**Findings** – The shrinkage rates of the tested specimens ranged from 15.5 to 20.4% along the length and width axis and 18.5% to 23.1% along the thickness axis of the specimens. Layer height and raster angle were the most statistically significant parameters influencing shrinkage, while print speed had very little influence. Three types of defects were observed, including surface roughness, surface deformation (warping and distortion) and balling defects.

**Originality/value** – This paper bridges an existing gap in MEX Steel 316L literature, with a focus on the relationship between MEX manufacturing parameters and subsequent shrinkage behaviour. This study provides an in-depth analysis of the relationship between manufacturing parameters – layer height, raster angle and print speed and subsequent shrinkage behaviour, thereby providing further information on the relationship between the former and the latter.

**Keywords** Steel, Material extrusion, Shrinkage, Manufacturing parameters, Print quality

**Paper type** Research paper

## 1. Introduction

As the material extrusion (MEX) additive manufacturing (AM) process continues to mature, the demand for MEX-fabricated metal parts has increased significantly in recent times. Hence, research efforts have been geared towards further improving the overall quality of MEX metal parts. These metal parts are initially produced as metal-polymer “green” parts and then subsequently subjected to the debinding and sintering (D&S) process to produce the final metal parts. Typically, 16%–23% shrinkage must be accounted for when designing metal parts for production via the MEX process, as the part will shrink accordingly in length, width and thickness. The sintering process involves substantial shrinkage of the “green” part depending on the material and the manufacturing process parameters (Ait-Mansour *et al.*, 2020; Loh and German, 1996). Hence, the optimal combination of manufacturing

---

© Solomon O. Obadimu and Kyriakos I. Kourousis. Published by Emerald Publishing Limited. This article is published under the Creative Commons Attribution (CC BY 4.0) licence. Anyone may reproduce, distribute, translate and create derivative works of this article (for both commercial and non-commercial purposes), subject to full attribution to the original publication and authors. The full terms of this licence may be seen at <http://creativecommons.org/licenses/by/4.0/legalcode>

*Declaration of competing interests:* The authors declare that they have no known competing financial interests or personal relationships that could have appeared to influence the work reported in this paper.

*CRediT authorship contribution statement:* (Solomon O. Obadimu): Conceptualization, methodology, software, validation, investigation, formal analysis, data curation, visualisation, writing – original draft, writing – review and editing. (Kyriakos I. Kourousis): Conceptualization, methodology, validation, investigation, formal analysis, visualisation, writing – review and editing, supervision, project administration, funding acquisition.

This work has been supported by the Faculty of Science and Engineering and the School of Engineering of the University of Limerick. Also, the financial support (Solomon O. Obadimu) received from the 2020 Government of Ireland Scholarship is acknowledged.

*Data availability:* The data used and/or analysed in the current study are contained within the manuscript or available from the corresponding author on reasonable request.

Received 8 July 2022

Revised 4 September 2022

Accepted 6 October 2022

---

The current issue and full text archive of this journal is available on Emerald Insight at: <https://www.emerald.com/insight/1355-2546.htm>



Rapid Prototyping Journal  
28/11 (2022) 92–101  
Emerald Publishing Limited [ISSN 1355-2546]  
[DOI 10.1108/RPJ-07-2022-0224]

parameters is paramount to reduce net shrinkage and also eliminate a source of distortion, thereby improving final MEX metal parts' quality and mechanical properties (Damon *et al.*, 2019; Loh and German, 1996).

Ample research studies have been devoted in studying the influence of MEX manufacturing parameters on subsequent mechanical performance. Using the steel 316L material, Kurose *et al.* (2020) established that varying build orientation induced mechanical and shrinkage anisotropy in MEX Steel 316L parts, reporting shrinkage values up to 15% along the x-y axis and up to 17% along the z-axis. Tosto *et al.* (2022), who varied layer height (LH), nozzle temperature and flow rate, similarly established the influence of manufacturing parameters on the mechanical performance of MEX Steel 316L. The authors found flow rate to have the most significant influence on the latter and specimen's density and porosity, reporting shrinkage ranging between 17 and 19% along the x-y axis and z axis, respectively. Caminero *et al.* (2021) reported an average anisotropic shrinkage ranging from 17.1 to 20.9% along the x to z axis, noting the influence of build orientation, print speed (PS) and LH on the former. Overall, they found specimens printed in the upright orientation exhibited a higher variability of shrinkage values compared to their counterparts – on-edge and flatwise-oriented specimens.

It is evident from the above that the varying MEX manufacturing processes indeed induce anisotropic shrinkage behaviours in MEX 316L parts. However, this important aspect of the MEX process has received limited attention in the published literature when compared to the more comprehensive studies on the influence of varying MEX production processes on subsequent mechanical performance of MEX Steel 316L (Caminero *et al.*, 2021; Kasha *et al.*, 2022; Kurose *et al.*, 2020). While shrinkage behaviours of Ultrafuse 316L parts have been well documented (as highlighted above), the effects of varying MEX manufacturing parameters on subsequent shrinkage behaviour have not been investigated in depth. Already published data on shrinkage behaviour are limited to the general shrinkage behaviours along the x-y (up to 18%) and z axes (up to 23%) (Gong *et al.*, 2019; Kurose *et al.*, 2020), without details on the relationship between shrinkage and the varying MEX manufacturing parameters. Wei *et al.* (2022) identified that primary manufacturing parameters, including build orientation, affect the shrinkage behaviour of MEX metal parts following their investigations on MEX bronze metal specimens. In this regard, to the authors' best knowledge, in-depth investigations into the influence of varying MEX manufacturing processes and subsequent shrinkage behaviour of MEX Steel 316L parts are currently limited to the works of Quarto *et al.* (2021) and Caminero *et al.* (2022).

Attempting to bridge the aforementioned gap in knowledge, Quarto *et al.* focused their research on studying the relationship between varying manufacturing parameters and the subsequent shrinkage behaviour of MEX Steel 316L parts, varying LHs (0.1 and 0.4 mm), infill patterns (wall and line), PSs (20 and 50 mm/s) and nozzle temperatures (170 and 240°C), keeping infill density and print bed temperature constant. The authors used the ANOVA statistical tool to study the relationship between the parameters and shrinkage behaviour, recommending the combination of 20 mm/s PS, 0.1 mm LH and line infill pattern. Caminero *et al.* (2022) similarly studied the relationship between

manufacturing parameters and subsequent shrinkage of Ultrafuse 316L samples, varying PS (30, 40 and 50 mm/s), LH (0.20 and 0.25 mm), build orientations (upright, on-edge and flat) and nozzle diameter (0.4 and 0.6 mm), whilst keeping infill density and pattern, nozzle temperature and print bed temperature constant. The authors used the artificial neural networks (ANNs) model to characterise and develop predictive models to estimate the shrinkage behaviour of the specimens. The ANN leverages machine learning to identify hidden patterns and links in a data set (Muhammad *et al.*, 2021). Following ANN characterisation, Caminero *et al.* found that build orientation, LH and PS had no significant effect on shrinkage rate. However, they found nozzle diameter to influence shrinkage behaviour, with specimens produced with 0.6 mm nozzle diameter exhibiting less shrinkage than their (0.4 mm nozzle) counterparts.

Besides the influence of varying production processes discussed above, the reproducibility of AM parts owing to the variation between Computer-aided design (CAD) drawings and fabricated parts continues to impede the further application of MEX metal parts (Obadimu and Kourousis, 2021), including those produced with the Ultrafuse Steel 316L material. Further research is necessary to improve dimensional control of these parts. As highlighted above, an appropriate selection of manufacturing parameters will reduce the overall shrinkage of MEX metal parts, subsequently improving the overall quality and the mechanical performance of the produced parts. However, considering the MEX metal part shrinkage, the identification and selection of manufacturing parameters capable to achieve a high-quality part poses a challenge. The aforementioned gap in knowledge offers an opportunity to conduct further investigations into the use of this material.

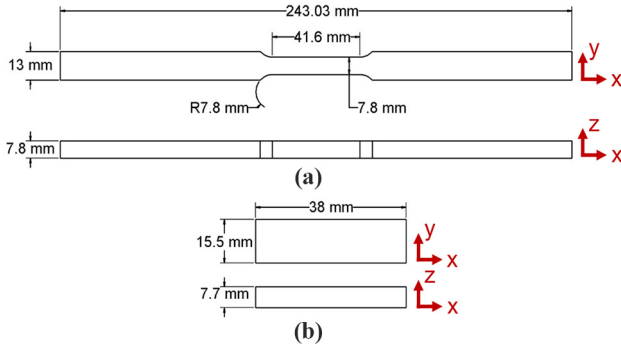
Considering the literature above, and building upon the current understanding of the MEX metal production process (Ait-Mansour *et al.*, 2020; Gong *et al.*, 2019; Obadimu *et al.*, 2021), this paper focuses on exploring the influence of manufacturing parameters, namely, PS, RA and LH on the MEX Ultrafuse Steel 316L shrinkage behaviour. ANOVA was used to study the relationship between these manufacturing parameters and shrinkage.

## 2. Materials and methods

### 2.1 Fabrication of specimens

A non-slip surface BASF Ultrafuse Steel 316L metal composite material with 90 vol% Steel 316L 1.75 mm diameter filament (BASF, 2021a, 2021b) was used for this research study. A total of 56 metal-polymer specimens (with varying manufacturing parameters), including 32 dog-bone and 24 rectangular specimens, have been examined in this study. The specimens were produced using the Prusa i3 MK3 machine via the G-code generated from the PrusaSlicer-2.3.1 software. It is noted that these specimens have been used in a separate research project investigating the tensile and flexural performance of the Ultrafuse Steel 316L material. Figure 1 shows the geometry and dimensions (x: length, y: width, z: thickness) of the "green" metal-polymer specimens. The dog-bone specimens were printed in flatwise orientation (xy build plate plane), while the rectangular specimens in flatwise (xy build plate plane) and on-edge orientation (xz build plate plane). The full set of printing parameters used is detailed in Tables 1 and 2.

**Figure 1** “Green” metal-polymer specimen geometry and dimensions (x: length, y: width, z: thickness)



Notes: (a) Dog-bone specimen; (b) rectangular specimen

**Table 1** Dog-bone specimens' fabrication parameters

Parameter	Value			
Print bed temperature [°C]	90			
Nozzle temperature [°C]	235			
Wall count/perimeters	2			
Infill type	Rectilinear (lines)			
Infill density [%]	100			
Fan speed [%]	50			
Extrusion multiplier	1			
LH [mm]	0.15	0.20	0.25	
PS [mm/s]	30	35	40	
RA [°]	±45			0/90

**Table 2** Rectangular specimens' fabrication parameters

Parameter	Value			
Print bed temperature [°C]	60			
Nozzle temperature [°C]	215			
Wall count/perimeters	2			
Infill type	Rectilinear (lines)			
Infill density [%]	100			
Fan speed [%]	100			
Extrusion multiplier	1			
PS [mm/s]	20			
LH [mm]	0.10	0.15	0.20	
RA [°]	±30	±45	±75	0/90

A total of 64 specimens were originally fabricated (printed), including 36 flatwise (tensile) dog-bone specimens and 24 flatwise flexural specimens, as well as 4 “on edge” orientation specimens, produced for a general flexural strength comparison, as detailed in the authors' paper (Kasha *et al.*, 2022). However, due to the rigorous D&S processing conditions, only 52 flatwise orientation specimens, including 32 dog-bone specimens and 20 flatwise orientation specimens, were deemed suitable for testing (inspected to be free of macro defects). Thus, some dog-bone specimens had three duplicates, while others had two, while some flexural specimens had two, while others had one. Nonetheless, a final total of 52 flatwise

orientation specimens were deemed sufficient to meet the objective of this research, i.e. investigating the influence of varying manufacturing parameters on subsequent shrinkage properties. The full mechanical properties analysis of the tensile specimens, and a separate set of flexural strength specimens, have been reported in two different publications. It is again noted that, as the premise of the authors' research was to focus only on the flatwise orientation specimen, the four on-edge flexural specimens were only used for a general comparison detailed in the authors' published paper (Kasha *et al.*, 2022).

Following the fabrication process, the “green” specimens were shipped to a BASF-approved D&S facility to obtain the final metal parts. The specimens were placed in the furnace in the thickness direction (z-direction) for the flat build orientation specimens, and in the width direction (y-direction) for the on-edge rectangular specimens. The green specimens were heated to a temperature of 110°C in a nitrogen environment whilst being exposed to nitric acid fumes until about 90% of the binder was removed. Following the debinding phase, brown porous specimens were obtained, with the remaining binder (approximately 10%) retaining each specimen's geometry. The specimens were subsequently exposed to a temperature of 600°C at 5 K/min for 1 h, removing the remaining binder, and then at 1,380°C for 3 h, fusing the metal particles and producing densified specimens.

## 2.2 Shrinkage characterisation

The length (x), width (y) and thickness (z) values of the “green” metal-polymer and the sintered metal specimens were measured using a high accuracy digital vernier calliper with a precision of 0.01 mm to perform shrinkage analysis. To reduce human error, three readings were taken for each dimension, and the averages were used to calculate the shrinkage rate (SR) using equation (1):

$$SR = \frac{S_{green} - S_{sintered}}{S_{green}} \% \quad (1)$$

where  $S_{green}$  the pre D&S (“green” part) specimen's dimension, and  $S_{sintered}$  the final (sintered part) specimen's dimension, along the x, y and z axes.

## 2.3 Design of experiment and statistical analysis

This paper is part of a larger study by the authors (Obadimu, 2022) on MEX Steel 316L and builds upon an already published paper (Kasha *et al.*, 2022). As a result, all the specimens used in our previous studies informed the design of experiment (DOE) matrix herein. The rectangular specimens emanate from the flexural bending paper (Kasha *et al.*, 2022), while the dog-bone specimens are from a tensile strength study by the authors, currently under review in another journal. However, due to the size (and word count limitation), the aforementioned papers could not be incorporated into the present manuscript. The tensile and flexural strength analyses DOEs were based on a literature survey in attempt to bridge identified gaps in relation to the influence of LH, PS and RA on mechanical properties. The full factorial DOE matrices for the dog-bone and the rectangular specimens, with all combinations of LH, PS and RA values, are shown in Tables 3 and 4, respectively.

**Table 3** Dog-bone specimens' DOE matrix showing the combinations of LH, PS and RA

DOE combinations [LH, PS, RA] LH in mm, PS in mm/s, Ra in °angle	
[0.15, 30, 0°/90°]	
[0.15, 35, 0°/90°]	[0.15, 35, ±45°]
[0.15, 40, 0°/90°]	[0.15, 40, ±45°]
[0.20, 35, 0°/90°]	
[0.20, 40, 0°/90°]	[0.20, 40, ±45°]
[0.25, 35, 0°/90°]	[0.25, 35, ±45°]
[0.25, 40, 0°/90°]	[0.25, 40, ±45°]

Note: The notation [LH, PS, RA] is used, where LH is given in mm, PS in mm/s and RA in °angle

**Table 4** Rectangular specimens' DOE matrix used in the present study showing the combinations of LH and RA

DOE combinations [LH, RA] LH in mm, RA in °angle	
<i>Flatwise</i>	
[0.10, ±30°]	[0.10, ±45°]
[0.15, ±30°]	[0.15, ±45°]
[0.20, ±30°]	[0.20, ±45°]
[0.10, ±75°]	[0.10, 0°/90°]
[0.15, ±75°]	[0.15, 0°/90°]
[0.20, ±75°]	[0.20, 0°/90°]
<i>On-edge</i>	
[0.10, ±35°]	
[0.15, ±45°]	
[0.20, 0°/90°]	

Note: The notation [LH, RA] is used, where LH is given in mm and RA in °angle

ANOVA investigates the statistical relationship between dependent (shrinkage rate) and independent variables (LH, RA and PS), as well as their interaction effects. Herein, the following possible effects were considered:

- the effect of each independent variable (manufacturing parameters) on the dependent variable (shrinkage properties); and
- the effects of their interaction on shrinkage properties.

The confidence level was set at 95%, i.e. 0.05 significance level, to facilitate these analyses. To eliminate any possibility of bias in the data sets, ensuring sufficient replicas of experimental data, the analysis for the 30 mm/s LH case for the dog-bone specimens and the “on-edge” case for the rectangular specimens, were removed from the ANOVA statistical analysis data. This was deemed necessary to estimate experimental variability, towards improving the accuracy of the analysis.

### 3. Results and discussion

#### 3.1 Shrinkage behaviour

The average shrinkage properties obtained from the different types of specimens are summarised in Tables 5 and 6,

**Table 5** Average shrinkage properties per tested type of Ultrafuse steel 316L dog-bone specimens for the different combinations of manufacturing parameters

Type of specimen	Shrinkage rate (%)		
	Length (x)	Width (y)	Thickness (z)
[0.15, 35, ±45°]	15.9 ± 0.2	18.3 ± 0.6	20.3 ± 0.8
[0.15, 40, ±45°]	16.0 ± 0.2	17.7 ± 0.6	19.9 ± 0.8
[0.20, 40, ±45°]	15.8 ± 0.2	18.1 ± 0.6	20.1 ± 0.8
[0.25, 35, ±45°]	15.9 ± 0.2	17.5 ± 0.6	18.6 ± 0.8
[0.25, 40, ±45°]	15.8 ± 0.2	17.1 ± 0.6	19.0 ± 0.8
[0.15, 30, 0°/90°]	15.5 ± 0.2	16.6 ± 0.5	20.3 ± 1.2
[0.15, 35, 0°/90°]	15.8 ± 0.2	17.4 ± 0.5	21.3 ± 1.2
[0.15, 40, 0°/90°]	15.8 ± 0.2	17.1 ± 0.5	21.3 ± 1.2
[0.20, 35, 0°/90°]	15.9 ± 0.2	16.9 ± 0.5	19.5 ± 1.2
[0.20, 40, 0°/90°]	15.9 ± 0.2	16.8 ± 0.5	19.9 ± 1.2
[0.25, 35, 0°/90°]	15.9 ± 0.2	16.8 ± 0.5	18.5 ± 1.2
[0.25, 40, 0°/90°]	16.0 ± 0.2	16.5 ± 0.5	18.6 ± 1.2

**Table 6** Average shrinkage properties per tested type of Ultrafuse steel 316L rectangular specimens (flatwise and on-edge orientation) for the different combinations of manufacturing parameters

Type of specimen	Shrinkage rate (%)		
	Length (x)	Width (y)	Thickness (z)
<i>Flatwise</i>			
[0.10, ±30°]	17.6 ± 0.3	18.2 ± 0.5	22.5 ± 0.7
[0.15, ±30°]	17.2 ± 0.3	18.9 ± 0.5	21.5 ± 0.7
[0.20, ±30°]	16.8 ± 0.3	17.2 ± 0.5	21.3 ± 0.7
[0.10, ±45°]	17.4 ± 0.3	17.8 ± 0.5	22.1 ± 0.7
[0.15, ±45°]	17.2 ± 0.3	18.2 ± 0.5	21.5 ± 0.7
[0.20, ±45°]	16.7 ± 0.3	17.5 ± 0.5	21.2 ± 0.7
[0.10, ±75°]	17.3 ± 0.3	18.2 ± 0.5	22.4 ± 0.7
[0.15, ±75°]	17.2 ± 0.3	18.0 ± 0.5	21.6 ± 0.7
[0.20, ±75°]	16.9 ± 0.3	17.2 ± 0.5	21.4 ± 0.7
[0.10, 0°/90°]	17.3 ± 0.3	18.3 ± 0.5	23.1 ± 0.7
[0.15, 0°/90°]	17.1 ± 0.3	17.8 ± 0.5	21.7 ± 0.7
[0.20, 0°/90°]	17.1 ± 0.3	18.5 ± 0.5	21.1 ± 0.7
<i>On-edge</i>			
[0.10, ±30°]	17.0 ± 0.2	20.4 ± 0.2	18.6 ± 0.6
[0.15, ±45°]	16.7 ± 0.2	20.0 ± 0.2	18.9 ± 0.6
[0.20, 0°/90°]	16.7 ± 0.2	20.2 ± 0.2	19.3 ± 0.6

namely, x (length), y (width) and z (thickness) shrinkage. All specimens exhibited anisotropic shrinkage behaviour, indicating a dependence of shrinkage behaviour on the MEX manufacturing parameters. The average percentage shrinkage ranged from 15.5 to 20.4% along the x and y axes, and 18.5 to 23.1% along the z axis. The dog-bone specimens experienced the lowest shrinkage along the x and y, and z axis at 15.5 and 18.5%, respectively. The rectangular specimens, on the other hand, accounted for 16.7 and 23.1% along the x and y, and z axis, respectively.

The %shrinkage along the z axis was the highest for all the specimens, as similarly reported in the published literature (Ait-Mansour *et al.*, 2020; Gong *et al.*, 2019; Kurose *et al.*, 2020;

Tosto *et al.*, 2021). Gong *et al.* attributed this to the effect of gravity on the specimens during the D&S process (Gong *et al.*, 2019), as the specimens were debound and sintered in the thickness direction (z-direction) for the flat build orientation specimens and in the width direction (y-direction) for the on-edge rectangular specimens, which justifies why the specimens experienced the highest shrinkage in their respective sintering directions/orientations.

3.2 ANOVA statistical analysis

The results presented in Section 3.1 indicate a dependence of shrinkage behaviour on MEX manufacturing parameters. Hence, to gain an insight into the relationship between the manufacturing parameters in focus and the resulting shrinkage of the MEX Ultrafuse Steel 316L specimens, an ANOVA statistical analysis has been performed on the dataset. The main effects plot of each parameter has been created, presented in Figure 2, to corroborate the ANOVA findings.

3.2.1 X-axis (length) shrinkage

The obtained ANOVA results for the x-axis (length) shrinkage versus LH, PS and RA are presented in Tables 7 and 8 for the dog-bone and rectangular specimens, respectively. The

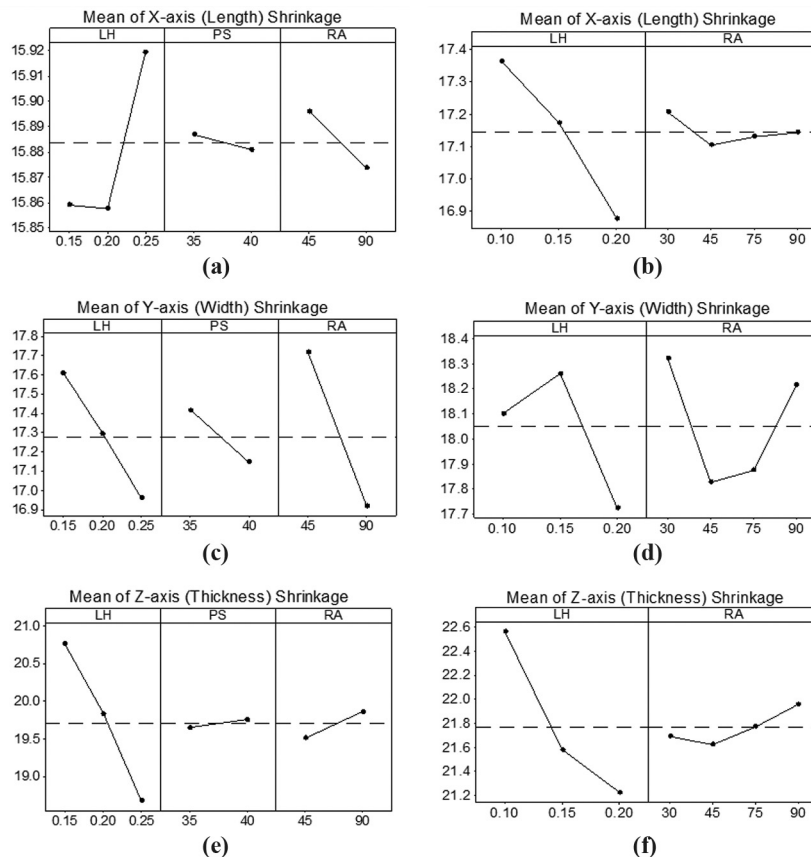
AVOVA results for the dog-bone specimens (Table 7) suggest that all the manufacturing parameters have no statistical significance on x-axis (length) shrinkage ( $p > 0.05$ ). In the case of the rectangular specimens, as evidenced in Table 8, interestingly, LH is found to have a statistical significance ( $p < 0.05$ ) on shrinkage, while RA shows no statistical significance. Regarding their interaction effect, ANOVA suggests there is no statistical significance between these parameters in both cases (i.e. the dog-bone and rectangular specimens).

The main effects plot provided in Figure 2(a) and 2(b) confirm the ANOVA results. For the rectangular specimens, the plots show that as LH increases from 0.10 to 0.20 mm, a reduction in shrinkage can be observed (from approximately 17.38 to approximately 16.87%). On the other hand, raster angle (RA) and PS show little or no effect on x-axis (length) shrinkage.

3.2.2 Y-axis (width) shrinkage

The ANOVA results for the y-axis (width) shrinkage are presented in Tables 9 and 10 for the dog-bone and rectangular specimens, respectively. Results presented in Table 9 show a significant effect of LH and RA on the y-axis (width) shrinkage for the dog-bone specimens, with RA being the most statistically significant, followed by LH. However, PS shows no

Figure 2 Main effect plots for the effect of manufacturing parameters (LH, PS and RA) on the shrinkage rate of the dog-bone and rectangular Ultrafuse Steel 316L specimens



Notes: (a) Dog-bone x-axis; (b) Rectangular x-axis; (c) Dog-bone y-axis; (d) Rectangular y-axis; (e) Dog-bone z-axis; (f) Rectangular z-axis

**Table 7** ANOVA results for the influence of x-axis (length) shrinkage of the Ultrafuse steel 316L dog-bone specimens from the fabrication parameters of LH, PS and RA

Parameter	Degree of freedom (DF)	Adjusted sums of squares (Adj SS)	Adjusted mean squares (Adj MS)	F-value	p-value
LH	2	0.02	0.01	0.27	0.77
PS	1	0.00	0.00	0.04	0.84
RA	1	0.00	0.00	0.07	0.79
LH*PS	2	0.02	0.01	0.30	0.75
LH*RA	2	0.16	0.08	2.60	0.10
PS*RA	1	0.01	0.01	0.18	0.67
Error	19	0.57	0.03	–	–
Lack of fit	1	0.03	0.03	1.03	0.32
Pure error	18	0.54	0.03	–	–
Total	28	0.80	–	–	–

**Table 8** ANOVA results for the influence of x-axis (length) shrinkage of the Ultrafuse steel 316L rectangular specimens from the fabrication parameters of LH and RA

Parameter	Degree of freedom (DF)	Adjusted sums of squares (Adj SS)	Adjusted mean squares (Adj MS)	F-value	p-value
LH	2	0.69	0.34	11.54	0.00
RA	3	0.03	0.01	0.30	0.83
LH*RA	6	0.22	0.04	1.24	0.38
Error	8	0.24	0.03	–	–
Total	19	1.21	–	–	–

**Table 9** ANOVA results for the influence of y-axis (width) shrinkage of the Ultrafuse steel 316L dog-bone specimens from the fabrication parameters of LH, PS and RA

Parameter	Degree of freedom (DF)	Adjusted sums of squares (Adj SS)	Adjusted mean squares (Adj MS)	F-value	p-value
LH	2	2.76	1.38	7.76	0.00
PS	1	0.54	0.54	3.02	0.10
RA	1	4.36	4.36	24.49	0.00
LH*PS	2	0.04	0.02	0.12	0.88
LH*RA	2	0.35	0.18	0.99	0.39
PS*RA	1	0.06	0.06	0.36	0.55
Error	19	3.38	0.18	–	–
Lack of fit	1	0.00	0.00	0.01	0.93
Pure error	18	3.38	0.19	–	–
Total	28	12.10	–	–	–

statistical significance ( $p > 0.05$ ) on shrinkage. In the case of the rectangular specimens, as evidenced in [Table 10](#), again, LH shows statistical significance, while ANOVA suggests RA is insignificant as a single parameter in this case. Regarding their interaction effect, ANOVA suggests there is no statistical significance ( $p > 0.05$ ) for the dog-bone specimens, while there is a significant interaction between LH and RA ( $p < 0.05$ ) for the rectangular specimens, suggesting that the influence of RA on the y-axis (width) shrinkage depends on the interaction between these two parameters, making RA equally significant.

The main effects plot in [Figure 2\(c\)](#) and 2(d) visually confirms the ANOVA results. In the case of the dog-bone specimens, it can be observed that as LH increased from

0.15 to 0.25 mm, the shrinkage rate reduced from approximately 17.68 to 16.9%, respectively. Similarly, a reduction in the y-axis (width) shrinkage can be observed as RA changed from  $\pm 45$  to  $0^\circ/90^\circ$ . A similar reduction in the y-axis (width) shrinkage rate can be observed in the case of the rectangular specimens.

### 3.2.3 Z-axis (thickness) shrinkage

The ANOVA results presented in [Table 11](#) suggest that LH, again, has a statistical significance on the z-axis (thickness) shrinkage, while RA and PS are statistically insignificant as a single parameter in the case of the dog-bone specimens. Similarly to the dog-bone, LH is also statistically significant

**Table 10** ANOVA results for the influence of y-axis (width) shrinkage of the Ultrafuse steel 316L rectangular specimens from the fabrication parameters of LH and RA

Parameter	Degree of freedom (DF)	Adjusted sums of squares (Adj SS)	Adjusted mean squares (Adj MS)	F-value	p-value
LH	2	1.48	0.74	6.66	0.02
RA	3	0.62	0.21	1.86	0.21
LH*RA	6	2.67	0.44	4.00	0.04
Error	8	0.89	0.11	–	–
Total	19	5.43	–	–	–

**Table 11** ANOVA results for the influence of z-axis (thickness) shrinkage of the Ultrafuse steel 316L dog-bone specimens from the fabrication parameters of LH, PS and RA

Parameters	Degree of freedom (DF)	Adjusted sums of squares (Adj SS)	Adjusted mean squares (Adj MS)	F-value	p-value
LH	2	23.53	11.77	57.35	0.00
PS	1	0.09	0.09	0.42	0.52
RA	1	0.25	0.25	1.23	0.28
LH*PS	2	0.27	0.14	0.66	0.53
LH*RA	2	2.91	1.46	7.10	0.00
PS*RA	1	0.00	0.00	0.00	0.98
Error	19	3.90	0.21	–	–
Lack of fit	1	0.20	0.20	0.97	0.34
Pure error	18	3.70	0.21	–	–
Total	28	33.23	–	–	–

( $p < 0.05$ ) in the case of the rectangular specimens (Table 12). Interestingly, regarding their interaction effects, ANOVA results suggest there is a significant interaction between LH and RA ( $p < 0.05$ ) for the dog-bone specimens, indicating that the effect of RA on the z-axis shrinkage is dependent on the interaction with LH. On the hand, in the case of the rectangular specimens, ANOVA results suggest there is no statistical significance ( $p > 0.05$ ) between the manufacturing parameters.

The main effects plot in Figure 2(e) and 2(f) visually confirms the ANOVA results. In the case of the dog-bone specimens, the plot shows that as LH increases from 0.15 to 0.25 mm, a reduction in shrinkage rate can be observed (from approximately 20.8 to 18.7%), while RA shows some significance due to its interaction effects with LH, and PS shows little or no effect on the z-axis (thickness) shrinkage. Regarding the rectangular specimens, similarly to their dog-bone counterparts, a reduction in the z-axis shrinkage can be observed (from approximately 22.6 to 21.2%) as LH increased from 0.10 to 0.20 mm.

### 3.2.4 Overall evaluation

Regarding shrinkage along the x-axis (length), the ANOVA results suggest that the three in-focus manufacturing parameters do not have a statistical significance on shrinkage rate for the dog-bone specimens. Whereas, LH is found to have a statistical significance on the x-axis shrinkage for the rectangular specimens. Regarding shrinkage along the y-axis (width), ANOVA results suggest that both LH and RA affect shrinkage rates along the y-axis (width) of the rectangular and dog-bone specimens. Similarly to the shrinkage rate along the y-axis, LH is found to be the most statistically significant factor for the two types of specimens in terms of shrinkage along the z-axis (thickness). Although ANOVA suggests that RA is statistically insignificant for the rectangular specimens, it is found to be a significant parameter due to its interaction effect with LH for the dog-bone specimens. In all cases, as evidenced in Tables 7 to 12, LH and RA have the most significant influence on the shrinkage rate of MEX Ultrafuse Steel 316L specimens, with LH topping the list. Whereas, PS showed little

**Table 12** ANOVA results for the influence of z-axis (thickness) shrinkage of the Ultrafuse steel 316L rectangular specimens from the fabrication parameters of LH and RA

Parameters	Degree of freedom (DF)	Adjusted sums of squares (Adj SS)	Adjusted mean squares (Adj MS)	F-value	p-value
LH	2	4.82	2.41	6.18	0.02
PA	3	0.34	0.11	0.29	0.83
LH*PA	6	0.72	0.12	0.31	0.92
Error	8	3.12	0.39	–	–
Total	19	10.04	–	–	–

or no influence on shrinkage rate within this experimental design (which corresponds to a subset of the broader range of acceptable set of parameters). While it is evident from the results presented above that MEX process parameters indeed influence the shrinkage properties of Steel 316L parts, interestingly, [Caminero et al. \(2022\)](#) found that build orientation, LH and PS had no significant effect on shrinkage rate, although, they found nozzle diameter to influence shrinkage behaviour. [Quarto et al. \(2021\)](#), on the other hand, found manufacturing parameters to influence each axis differently, with PS topping the list, followed by LH and nozzle temperature.

The difference in the statistical significance of LH on the x-axis (length) shrinkage and the difference in the trend observed in the RA main effect plots ([Figure 2](#)), between the dog-bone and rectangular specimens, may be attributed to the specimens' different size and geometry, as well as the varying D&S processing conditions. BASF ([BASF, 2021b](#)) stresses that "the goal of debinding is to remove the binder in the shortest amount of time with the least impact on the final part", highlighting that the larger the green part, the longer the production process ([BASF, 2021b](#)). This infers that the longer production process for the dog-bone specimens (due to their larger size than rectangular specimens) may have induced the difference in the effect of LH observed along the x-axis, as well as the difference in the RA trends observed in [Figure 2](#).

Regarding the relationship between MEX Ultrafuse Steel 316L parts' shrinkage and their subsequent mechanical properties, it is noteworthy to mention that the ANOVA findings reported above are in good agreement with the ANOVA findings in a paper by the authors, currently under review in a different journal. In the paper, LH and RA were similarly found to be the most statistically significant manufacturing parameters, with LH also topping the list. These findings suggest that there is a potential connection between the shrinkage of Ultrafuse Steel 316L specimens and their subsequent tensile mechanical performance. [Kościszko et al. \(2021\)](#) studied the effect of varying post-processing parameters (including conditioning time and temperature) on the shrinkage and mechanical performance of polypropylene specimens. Their experimental findings confirm that changes in post-processing temperature and conditions lead to changes in microstructure characteristics, which effectively induces shrinkage and mechanical anisotropy. [Huang and Hsu \(2011\)](#) also affirm that sintering temperature indeed affects dimensional shrinkage rate and the overall quality of sintered parts, including their mechanical performance. This may have been the case during the D&S process of the Ultrafuse Steel 316L specimens. Besides AM-induced microstructural heterogeneities, variability in D&S post-processing conditions, including handling and variations in processing temperature, may have further induced shrinkage and mechanical anisotropy in the Ultrafuse Steel 316L specimens, as presented above. [Askari et al. \(2019\)](#) asserted that a well-controlled D&S process is crucial to achieving excellent part quality.

### 3.3 Macroscopic examination of specimens

#### 3.3.1 Print quality

Residual stresses have been reported to affect the print quality of MEX parts. [Casavola et al. \(2017\)](#) pointed out that

managing residual stresses will reduce warping effects, a common fabrication challenge during MEX metal fabrication. While high temperatures are recommended for the Ultrafuse Steel 316L filament to facilitate better adhesion to the print bed, a point to highlight is its impact on the print surface. In the present study, the effects of print nozzle temperature and bed temperature on the print quality have also been evaluated. The former and latter were kept constant at 235 and 90°C, respectively, for the dog-bone specimens, and 215 and 60°C for the rectangular specimens.

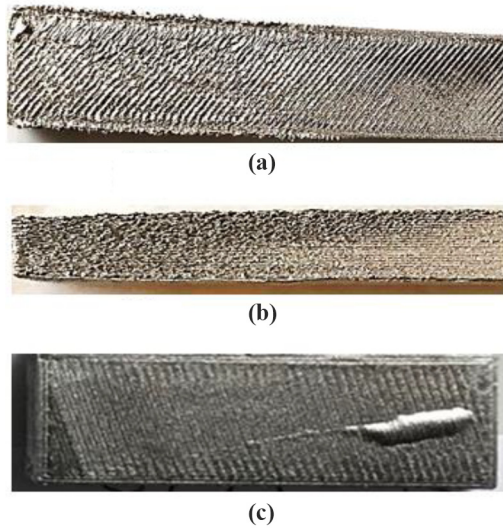
For the dog-bone specimens, following each production process, an uneven/undulating surface was observed at the periphery of each specimen, decreasing the adhesion forces between the specimen and the print bed. This effect was not observed while printing the rectangular specimens. Besides the high temperatures requirements of the Ultrafuse Steel 316L material (for both the nozzle and print bed), the undulating surface effect may be attributed to the long printing duration of the dog-bone specimens, up to 210 min for the former and up to 92 min for the rectangular specimens. Interestingly, [El Moumen et al. \(2019\)](#) noted that stress magnitude increases with printing time, i.e. the longer the printing time, the more the temperature drops and the higher the residual stresses and vice versa. According to the authors, temperature drops and changes as the filaments are deposited, generating a temperature gradient during the process, thereby increasing the concentration of stresses within each specimen during fabrication. Also, the specimen geometry and the motion pattern of the print nozzle (extrusion head) have been reported to influence the cooling rate of the specimens during production ([Sun et al., 2008](#)). Print nozzle travelling a long path length (dog-bone specimen) during fabrication leads to significant temperature fluctuations compared to travelling a short path length (rectangular specimens). As a result, the temperature gradient is lower for rectangular specimens because of the short travel path of the nozzle.

#### 3.3.2 Defects characterisation

All the specimens were visually inspected in their "green" state and following the D&S process, with the most commonly observed defects (post-sintering) illustrated in the images of [Figure 3\(a\)](#) to [3\(c\)](#). In particular, surface roughness, surface deformation (warping and distortion) and balling have been observed. Regarding the surface roughness and surface deformation defects, it is noted that these defects were visible on some specimens immediately after printing and further exacerbated during D&S, while the balling defect was only induced during the D&S process. Thus, it can be concluded that the surface roughness and surface deformation defects stem from the fabrication process and are further exacerbated during the D&S process, while the balling defect emanates from the D&S process.

[Malekipour and El-Mounayri \(Malekipour and El-Mounayri, 2018\)](#), who reviewed and classified common AM defects, classified these defects as surface quality (finishing) defects. The authors highlighted that surface roughness [[Figure 3\(a\)](#)] decreases with an increase in PS and vice versa, while they attributed surface deformation (warping and distortion) [[Figure 3\(b\)](#)] to residual stresses and the thermal gradient between layers/print zones with higher temperatures and layers/zones with lower temperatures.

**Figure 3** Most commonly observed defects in the Ultrafuse Steel 316L specimens following D&S process



**Notes:** (a) Surface roughness; (b) warping and distortion; (c) balling

Balling [Figure 3(c)], on the other hand, is one of the most common and referenced defects in AM (Malekipour and El-Mounayri, 2018). Balling occurs due to the “solidification of melted material into spheres due to instability in the melt pool surface tension, and wetting dynamics”, resulting in poor surface finish quality (Montazeri, 2019). In the case of the ME metal production process, as previously highlighted, variability in the D&S processing conditions, including variations in processing temperature, particularly during the sintering process when the specimens are exposed to up to 1,380°C to facilitate the solidification of the steel 316L metal particles may have induced the balling defect.

Overall, the observations presented above infer that macroscopic defects can be controlled to an extent as they emanate from the fabrication process. Besides increasing PS and reducing thermal gradient between layers/print zones during fabrication as noted by Malekipour and El-Mounayri (Malekipour and El-Mounayri, 2018), it is also imperative to ensure that the printing material does not clog up the nozzle during the fabrication process. As a result, adjusting the gap between the nozzle tip and the print bed for good adhesion to the print bed before the printing/fabrication process is recommended. This approach was found to affect print quality as a clogged nozzle limits the extrusion of the filament. More so, adhesion to the print bed is enhanced if the nozzle is adjusted, thereby improving the overall print quality.

#### 4. Conclusions

The shrinkage behaviour of the MEX Ultrafuse Steel 316L specimens has been investigated in this study. The ANOVA statistical tool was used to study the relationship between the main manufacturing parameters and the resulting shrinkage of the specimens. Furthermore, following the D&S process, the

most commonly observed defects have been characterised. The key conclusions drawn from this research are:

- The shrinkage behaviour of MEX Ultrafuse Steel 316L specimens is dependent on the manufacturing parameters, inducing anisotropic shrinkage behaviour in the specimens, similarly reported by Quarto *et al.* (2021), who observed that the relative density and shrinkage of MEX Steel 316L part is dependent on the process parameters. The shrinkage rates of the specimens ranged from 15.5 to 20.4% along the x-y axis and 18.5 to 23.1% along the z-axis.
- From the ANOVA statistical results, LH and RA were found to be the most statistically significant manufacturing parameters influencing the shrinkage behaviour of the MEX Ultrafuse Steel 316L specimens, while PS was found to have little or no influence on the shrinkage behaviour (within the experimental design). Quarto *et al.* (2021) similarly established the influence of MEX parameters on subsequent shrinkage behaviour of Steel 316L specimens, while Caminero *et al.* (2022) found varying manufacturing parameters to have a negligible influence on shrinkage rate.
- Three types of defects were observed in the specimens, including surface roughness, surface deformation (warping and distortion) and balling defects, with the latter induced during the D&S process and surface roughness and deformation emanating from the fabrication process.

#### References

- Ait-Mansour, I., Kretzschmar, N., Chekurov, S., Salmi, M. and Rech, J. (2020), “Design-dependent shrinkage compensation modeling and mechanical property targeting of metal FFF”, *Progress in Additive Manufacturing*, Vol. 5 No. 1, pp. 51–57, doi: [10.1007/s40964-020-00124-8](https://doi.org/10.1007/s40964-020-00124-8).
- Askari, A., Alaei, M.H., Nekouee, K., Mehdipoor Omrani, A. and Park, S.J. (2019), “The effect of debinding and sintering parameters on the mechanical and microstructural properties of Fe-2Ni metal injection molded compacts”, *Materials Research Express*, Vol. 6 No. 11, p. 1165e8, doi: [10.1088/2053-1591/ab4f26](https://doi.org/10.1088/2053-1591/ab4f26).
- BASF (2021a), “Ultrafuse® metal filaments technical data sheet for 3D printing metal parts”, available at: [https://forward-am.com/wp-content/uploads/2021/01/Ultrafuse\\_316L\\_TDS\\_EN\\_v1.1.pdf](https://forward-am.com/wp-content/uploads/2021/01/Ultrafuse_316L_TDS_EN_v1.1.pdf)
- BASF (2021b), “Ultrafuse® metal filaments user guidelines for 3D printing metal parts”, available at: [https://forward-am.com/wp-content/uploads/2021/04/UserGuidelines\\_2021\\_03\\_29.pdf](https://forward-am.com/wp-content/uploads/2021/04/UserGuidelines_2021_03_29.pdf)
- Caminero, M.Á., Gutiérrez, A.R. and Chac, J.M. (2022), “Effects of fused filament fabrication parameters on the manufacturing of 316L stainless-steel components: geometric and mechanical properties”, *May*, doi: [10.1108/RPJ-01-2022-0023](https://doi.org/10.1108/RPJ-01-2022-0023).
- Caminero, M.Á., Romero, A., Chacón, J.M., Núñez, P.J., García-Plaza, E. and Rodríguez, G.P. (2021), “Additive manufacturing of 316L stainless-steel structures using fused filament fabrication technology: mechanical and geometric properties”, *Rapid Prototyping Journal*, Vol. 27 No. 3, pp. 583–591, doi: [10.1108/RPJ-06-2020-0120](https://doi.org/10.1108/RPJ-06-2020-0120).

- Casavola, C., Cazzato, A., Moramarco, V. and Pappaletta, G. (2017), “Residual stress measurement in fused deposition modelling parts”, *Polymer Testing*, Vol. 58, pp. 249-255, doi: [10.1016/j.polymertesting.2017.01.003](https://doi.org/10.1016/j.polymertesting.2017.01.003).
- Damon, J., Dietrich, S., Gorantla, S., Popp, U., Okolo, B. and Schulze, V. (2019), “Process porosity and mechanical performance of fused filament fabricated 316L stainless steel”, *Rapid Prototyping Journal*, Vol. 25 No. 7, pp. 1319-1327, doi: [10.1108/RPJ-01-2019-0002](https://doi.org/10.1108/RPJ-01-2019-0002).
- El Moumen, A., Tarfaoui, M. and Lafdi, K. (2019), “Modelling of the temperature and residual stress fields during 3D printing of polymer composites”, *The International Journal of Advanced Manufacturing Technology*, Vol. 104 Nos 5/8, pp. 1661-1676, doi: [10.1007/s00170-019-03965-y](https://doi.org/10.1007/s00170-019-03965-y).
- Gong, H., Snelling, D., Kardel, K. and Carrano, A. (2019), “Comparison of stainless steel 316L parts made by FDM- and SLM-based additive manufacturing processes”, *JOM*, Vol. 71 No. 3, pp. 880-885, doi: [10.1007/s11837-018-3207-3](https://doi.org/10.1007/s11837-018-3207-3).
- Huang, M.-S. and Hsu, H.-C. (2011), “Influence of injection moulding and sintering parameters on properties of 316L MIM compact”, *Powder Metallurgy*, Vol. 54 No. 3, pp. 299-307, doi: [10.1179/003258909X12502679013819](https://doi.org/10.1179/003258909X12502679013819).
- Kasha, A., Obadimu, S.O. and Kourousis, K.I. (2022), “Flexural characteristics of material extrusion steel 316L: influence of manufacturing parameters”, *Additive Manufacturing Letters*, p. 100087, doi: [10.1016/j.addlet.2022.100087](https://doi.org/10.1016/j.addlet.2022.100087).
- Kościszko, A., Marciniak, D. and Sykutera, D. (2021), “Post-processing time dependence of shrinkage and mechanical properties of injection-molded polypropylene”, *Materials*, Vol. 14 No. 1, p. 22, doi: [10.3390/ma14010022](https://doi.org/10.3390/ma14010022).
- Kurose, T., Abe, Y., Santos, M.V.A., Kanaya, Y., Ishigami, A., Tanaka, S. and Ito, H. (2020), “Influence of the layer directions on the properties of 316L stainless steel parts fabricated through fused deposition of metals”, *Materials*, Vol. 13 No. 11, p. 2493, doi: [10.3390/ma13112493](https://doi.org/10.3390/ma13112493).
- Loh, N.H. and German, R.M. (1996), “Statistical analysis of shrinkage variation for powder injection molding”, *Journal of Materials Processing Technology*, Vol. 59 No. 3, pp. 278-284, doi: [10.1016/0924-0136\(95\)02158-2](https://doi.org/10.1016/0924-0136(95)02158-2).
- Malekipour, E. and El-Mounayri, H. (2018), “Common defects and contributing parameters in powder bed fusion AM process and their classification for online monitoring and control: a review”, *International Journal of Advanced Manufacturing Technology*, Vol. 95 Nos 1/4, pp. 527-550, doi: [10.1007/s00170-017-1172-6](https://doi.org/10.1007/s00170-017-1172-6).
- Montazeri, M. (2019), “Smart additive manufacturing: in-process sensing and turing: in-process sensing and data analytics for online defect detection in metal additive manufacturing processes turing processes”, [University of Nebraska – Lincoln], available at: <https://digitalcommons.unl.edu/mechengdiss/148/>
- Muhammad, W., Brahme, A.P., Ibragimova, O., Kang, J. and Inal, K. (2021), “A machine learning framework to predict local strain distribution and the evolution of plastic anisotropy & fracture in additively manufactured alloys”, Vol. 136, (September 2020), pp. 1-29, doi: [10.1016/j.ijplas.2020.102867](https://doi.org/10.1016/j.ijplas.2020.102867).
- Obadimu, S.O. (2022), “Material extrusion additive manufacturing of steel 316L: mechanical properties’ optimisation and the effect of load rate on in-plane compressive performance of honeycomb structures”, PhD Thesis, University of Limerick, Limerick, Ireland.
- Obadimu, S.O. and Kourousis, K.I. (2021), “Compressive behaviour of additively manufactured lattice structures: a review”, *Aerospace*, Vol. 8 No. 8, p. 207, doi: [10.3390/aerospace8080207](https://doi.org/10.3390/aerospace8080207).
- Obadimu, S.O., McLaughlin, J. and Kourousis, K. (2021), “Immersion ultrasonic testing of artificially induced defects in fused filament fabricated steel 316L”, *3D Printing and Additive Manufacturing*, pp. 1-6, doi: [10.1089/3dp.2021.0095](https://doi.org/10.1089/3dp.2021.0095).
- Quarto, M., Carminati, M. and D’Urso, G. (2021), “Density and shrinkage evaluation of AISI 316L parts printed via FDM process”, *Materials and Manufacturing Processes*, Vol. 36 No. 13, pp. 1535-1543, doi: [10.1080/10426914.2021.1905830](https://doi.org/10.1080/10426914.2021.1905830).
- Sun, Q., Rizvi, G.M., Bellehumeur, C.T. and Gu, P. (2008), “Effect of processing conditions on the bonding quality of FDM polymer filaments”, *Rapid Prototyping Journal*, Vol. 14 No. 2, pp. 72-80, doi: [10.1108/13552540810862028](https://doi.org/10.1108/13552540810862028).
- Tosto, C., Tirillò, J., Sarasini, F. and Cicala, G. (2021), “Hybrid metal/polymer filaments for fused filament fabrication (FFF) to print metal parts”, *Applied Sciences (Switzerland)*, Vol. 11 No. 4, p. 1, doi: [10.3390/app11041444](https://doi.org/10.3390/app11041444).
- Tosto, C., Tirillò, J., Sarasini, F., Sergi, C. and Cicala, G. (2022), “Fused deposition modeling parameter optimization for cost-effective metal part printing”, *Polymers*, Vol. 14 No. 16, p. 3264, doi: [10.3390/polym14163264](https://doi.org/10.3390/polym14163264).
- Wei, X., Behm, I., Winkler, T., Scharf, S., Li, X. and Bähr, R. (2022), “Experimental study on metal parts under variable 3D printing and sintering orientations using bronze/PLA hybrid filament coupled with fused filament fabrication”, *Materials*, Vol. 15 No. 15, p. 5333, doi: [10.3390/ma15155333](https://doi.org/10.3390/ma15155333).

### Corresponding author

Kyriakos I. Kourousis can be contacted at: [kyriakos.kourousis@ul.ie](mailto:kyriakos.kourousis@ul.ie)